ACS Photonics

pubs.acs.org/journal/apchd5

Letter

Plasmon-Mediated Coherent Superposition of Discrete Excitons under Strong Exciton−Plasmon Coupling in Few-Layer MoS_2 at Room Temperature

Aaron H. Rose,* Jeremy R. Dunklin, Hanyu Zhang, Juan M. Merlo, and Jao van de Lagemaat*

Cite This: *ACS Photonics* 2020, 7, 1129−1134

Read Online

ACCESS | Metrics & More | Article Recommendations | Supporting Information

ABSTRACT: We demonstrate room temperature coherent hybridization of the A- and B-excitons in few-layer MoS_2, mediated by simultaneous strong coupling to surface plasmon polaritons. Few-layer MoS_2 was placed on a tunable plasmonic structure and the system's dispersion was measured by tuning the plasmon energy across the exciton energies. Strong coupling was observed as double Rabi splitting at the A- and B-excitons of 81 and 93 meV, respectively. A coupled harmonic oscillator model sheds light on the nature of the interaction, revealing a quantum superposition of the A- and B-excitons, mediated by the plasmon interaction. This observation suggests the possibility of room temperature intra- or intervalley quantum information transport and/or spin entanglement. The experiment confirms a previous theoretical prediction of room temperature exciton−exciton hybridization in two-dimensional MoS_2. Further, through modeling we find that room temperature strong coupling is a general phenomenon among two-dimensional transition metal dichalcogenide exciton−plasmon systems.

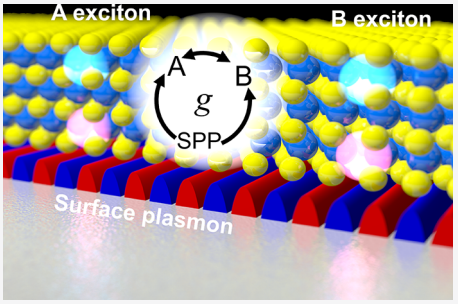

KEYWORDS: *strong coupling, two-dimensional system, transition metal dichalcogenide, MoS_2, surface plasmon polariton, exciton*

Two-dimensional transition metal dichalcogenides (2D TMDCs) are under intense study for their optical, electronic, and catalytic properties.[1−4] In particular, 2D TMDCs are a prime platform for studying coherent light−matter interactions, exhibiting strong room temperature exciton−polariton coupling due to their sharp excitonic transitions. Further, their nanometer thickness is suited for coupling to plasmon polaritons, being thinner than the plasmon optical near-field. While most strong coupling work has focused on coupling the A-exciton of monolayer TMDCs to polaritons, we find that simultaneous coupling to the B-exciton is possible at room temperature in few-layer MoS_2, allowing for hybridization of the two excitons.

Exciton−polariton strong coupling[5] has been studied in the field of cavity quantum electrodynamics for over three decades.[6] The field has produced many exciting observations such as thresholdless lasing,[7,8] room temperature condensation,[8] and other quantum coherent phenomena,[9] with potential applications in quantum information.[10−12] Strong coupling occurs between an electronic transition and an optical mode of equal energy when the coupling strength between the two is similar to or greater than their average decay.[10,13] Distinct from the weak coupling regime, where the Purcell effect[14] can modify the spontaneous emission rate, the energy band splitting that occurs under strong coupling conditions implies fundamentally new optoelectronic and chemical properties.[15] The band reconfiguration under strong coupling has been used to modify decay pathways and control chemical reaction rates in light-sensitive organic molecules.[15−17]

In 1974, Agranovich and Malshukov[18] predicted and in 1978 Pockrand and Swalen[19] demonstrated that the cavity polaritons can be replaced by surface plasmon polaritons to create exciton−plasmon strong coupling, opening up a new platform for strong coupling investigations. A wide array of plasmonic thin films and nanostructures is available to experimentalists[20] and allows for the excitonic system to be incorporated in a convenient open planar geometry. To date, most exciton−plasmon strong coupling has been demonstrated with organic dye molecules or quantum dots[13,20−22] due to their sharply defined exciton transitions, which survive at room temperature, and the ability to create thin films in the plasmon near field. Conventional inorganic semiconductors have exciton binding energies of ∼10 meV in the bulk[23] and a few times higher in two-dimensions,[24] near the thermal energy at room temperature of 26 meV and thus are generally cooled to observe strong coupling. More recently, 2D TMDCs have emerged as a new class of inorganic semiconductors with large binding

Received: March 13, 2020
Published: April 7, 2020

https://dx.doi.org/10.1021/acsphotonics.0c00233
ACS Photonics 2020, 7, 1129−1134

energies of ~100s of meV at mono- to few-layer thickness,[1] allowing strong coupling to be observed up to room temperature.[25] Further, their large absorption coefficients allow nanometer films to absorb tens of percent of incident light,[1] suitable for placement within the plasmon penetration depth, allowing for strong coupling studies with plasmon polaritons in addition to the conventional cavity polaritons.[25−29]

In this article, we demonstrate room temperature exciton−plasmon polariton strong coupling of the A- and B-excitons and A−B exciton−exciton hybridization in few-layer MoS_2 (FL-MoS_2) on thin Ag films. The observations of room temperature exciton−polariton strong coupling of the B-exciton in MoS_2 and room temperature exciton−exciton hybridization in any 2D TMDC has not been previously reported. Evidence for the strong coupling is found as double Rabi splitting at the A- and B-excitons in the experimental dispersion relation of 81 and 93 meV, respectively. A coupled harmonic oscillator model sheds light on the nature of the interaction and reveals a coherent quantum superposition of the A- and B-excitons, mediated by the plasmon interaction. We also show that room temperature strong coupling appears to be a general phenomenon in 2D TMDC exciton−plasmon systems by calculating dispersion plots for many systems in the Kretschmann-Raether configuration. Further, this is the first work to apply the Kretschmann-Raether configuration to strong plasmon coupling in the 2D TMDCs. The results obtained are important to the understanding of the properties of MoS_2 and other 2D TMDCs and could have implications in the design of polaritonic and valleytronic devices.

To study FL-MoS_2−Ag strong coupling, we employed the simple Kretschmann-Raether configuration, shown in Figure 1a, used in the pioneering exciton−plasmon coupling experiments.[19,30,31] The Kretschmann-Raether method[32] for exciting surface plasmons in a planar thin film offers a simple method to incorporate a tunable plasmon resonance and observe strong coupling. Detuning of the coupling (i.e., probing the interaction at energies away from that of maximum coupling) is achieved by simply varying the incident angle of light through the prism, allowing dispersion plots to be obtained in a straightforward manner. Transfer matrix simulations[33] used to find target values for the thickness of the Ag and MoS_2 layers showed that similar plasmon and exciton peak sizes are needed to optimize strong coupling;[34] ~40 nm Ag and few-layer-thick MoS_2 were found to be most favorable. The studied sample consisted of 15 nm CVD-grown FL-MoS_2 on 40 nm Ag on a glass prism. Further details of the fabrication and simulations are provided in the Supporting Information.

Evidence for strong coupling can be found as anticrossing, or Rabi splitting,[10] of the coupled modes in energy-momentum dispersion plots. Dispersion plots were constructed by collecting angle-resolved reflectance spectra in the Kretschmann-Raether configuration (Figure 1a) using an ellipsometer. Figure 1b shows the reflectance at a few incident angles, θ_e = 45°, 52°, and 60°. The plasmon energy blue shifts with increasing angle, dominating the spectrum at the largest and smallest angles and completely hybridizing with the excitons at the intermediate angle. Color dispersion plots were constructed by plotting absorptivity, A, as a function of incident photon energy, E, and in-plane wavevector, $k_{\|}$. Absorptivity was calculated as $A = 1 - R$, where R is reflectance. Transmission was assumed zero as incident light in the prism undergoes total internal reflection. Although the reflectance

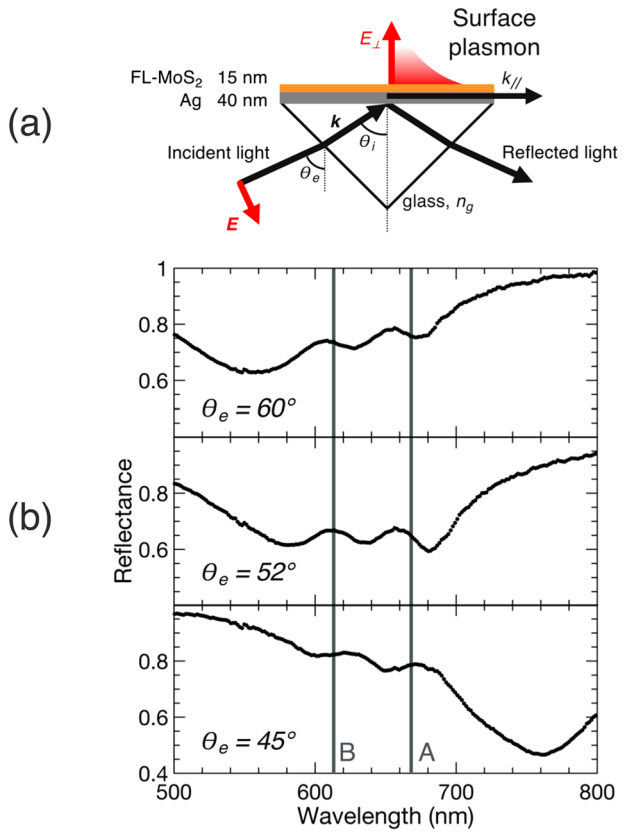

Figure 1. Plasmon excitation and angle-resolved reflectance using the Kretschmann-Raether method: (a) The plasmon is excited via p-polarized white light incident on the FL-MoS_2−Ag thin film through the backside of the glass prism. (b) Reflectance data at a few incident angles. The vertical gray lines mark positions of the uncoupled A- and B-excitons. At θ_e = 45° the plasmon is resonant at 760 nm and the exciton positions are slightly blue-shifted. In the vicinity of the exciton energies (θ_e = 52°), the plasmon completely hybridizes with the excitons. At θ_e = 60° the plasmon is resonant at 560 nm and the exciton positions are slightly red-shifted.

data is collected as a function of angle, the in-plane wavevector is the appropriate basis to use when studying strong coupling; using energy-angle dispersion plots results in an overestimation of the Rabi splitting energy.[13,35] The in-plane wavevector is calculated as $k_{\|} = (2\pi/\lambda)n_g\sin(\theta_i)$, where λ is the incident photon wavelength, n_g is the index of refraction of the prism, and θ_i is the incident angle of light inside the prism. All measurements were performed at room temperature in air. Further details of the measurement method are provided in the Supporting Information.

The experimentally determined dispersion of the few-layer MoS_2−Ag system is presented in Figure 2a. Avoided crossing and thus Rabi splitting is evident at both the uncoupled A- and B-exciton energies of 1.86 and 2.01 eV, respectively, indicating strong coupling between the surface plasmon and each exciton. The uncoupled exciton energies were determined from dips in the reflection spectrum taken from the air side of the prism, where coupling to the surface plasmon is disallowed. Among the 2D TMDC exciton−plasmon strong coupling literature, there has been limited work with MoS_2 at room temperature.[28,36] Liu et al. showed exciton−plasmon strong coupling in monolayer MoS_2 for both the A- and B-excitons at 77 K and for the A-exciton only at room temperature using a Ag nanodisk array.[28] Vasilevskiy et al. predicted strong room

https://dx.doi.org/10.1021/acsphotonics.0c00233
ACS Photonics 2020, 7, 1129−1134

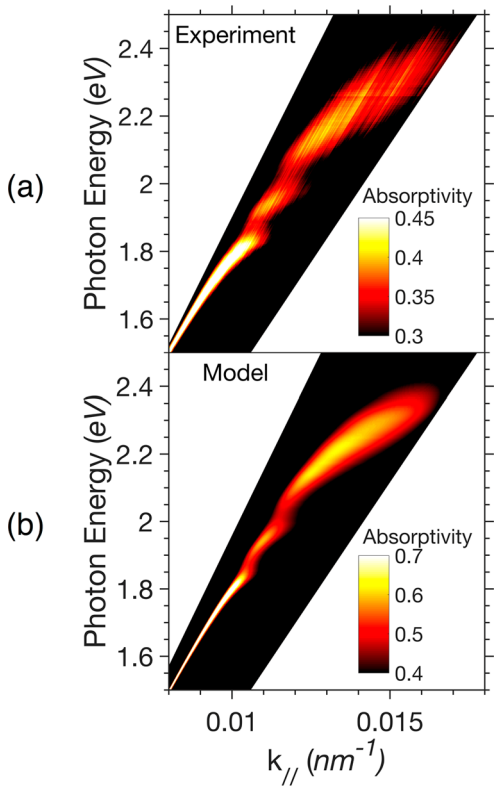

Figure 2. Dispersion of FL-MoS_2–Ag: (a) Experimental energy vs transverse wavevector dispersion obtained from angle-resolved reflectance. Rabi splitting of 81 and 93 meV is evident at the A- and B-exciton energies of 1.86 and 2.01 eV, respectively. (b) Modeled dispersion of the sample measured in panel a, calculated using the transfer matrix method. See main text for calculation of $k_{\|}$ and other quantities.

temperature coupling of the A- and B-excitons in both MoS_2 and WS_2 monolayers in cavities.[37] To the best of our knowledge, room temperature exciton–plasmon strong coupling of the B-exciton in MoS_2 has not been previously reported.

In Figure 2b, a transfer matrix model[33] shows good agreement with the data presented in Figure 2a. The thickness and complex refractive index of the Ag and MoS_2 thin films were measured with ellipsometry from the air side of a Ag control and the actual sample, respectively, and used in the model (see Supporting Information for further details of the model). In Figure 2a,b, the lack of data (white space) is a consequence of converting the dispersion plots from energy-angle to energy-momentum space, where $k_{\|} \sim \lambda^{-1} \sim E$, where E is the incident photon energy. The anticrossings do not quite go to zero because of an absorption background as well as overlap of the plasmon and exciton spectral shapes.

The strong coupling results in a dispersion with three branches with each branch representing a new hybrid exciton–plasmon mode, retaining some character of each of its constituent parts. It is expected that the new quasiparticles, which are discovered by their new optical properties, should also possess altered electrical and chemical behavior. Study of such properties is the subject of ongoing study. To gain further insight into the character of the three optical modes, we fit the data to a semiclassical coupled oscillator model and extracted the exciton and plasmon fraction of each mode.

The Hamiltonian representing the system in the coupled oscillator model is shown in eq 1.

$$\begin{pmatrix} E_{SPP}(k_{\|}) & \frac{\Omega_A}{2} & \frac{\Omega_B}{2} \\ \frac{\Omega_A}{2} & E_A & 0 \\ \frac{\Omega_B}{2} & 0 & E_B \end{pmatrix} \quad (1)$$

The semiclassical coupled oscillator model treats the problem as a three-level quantized system of classical fields where a full quantum model would use quantized fields. Both models give the same result for the Rabi splitting.[13] Loss is neglected and coupling between the A- and B-excitons is assumed zero (off diagonal zeros). The diagonal elements Ω_A and Ω_B are the Rabi splitting energies at the A- and B-excitons, equal to twice the coupling strength, $\Omega = 2g$. E_A and E_B are the uncoupled exciton energies. To fit the model to the data in Figure 2a, the peak positions of the three branches were found by fitting the absorptivity $A(E)$ at each $k_{\|}$ to three Lorentzians, represented by the black data in Figure 3. For the fit, Ω_A, Ω_B, E_A, and E_B are set as fit parameters. As such, the only input into eq 1 is $E_{SPP}(k_{\|})$, the uncoupled plasmon energy. However, the plasmon dispersion from a control sample with no MoS_2 does not accurately represent the uncoupled plasmon energy of a sample with MoS_2 because the media on both sides of the metal thin film influence the behavior of the surface plasmon. Particularly, the real part of the MoS_2 refractive index controls the behavior of the plasmon in the same way the addition of a lossless dielectric thin film would. The imaginary part is responsible for the exchange of energy and thus controls the coupling. To this end, the transfer matrix model from Figure 2b is solved again, but with the imaginary part of the MoS_2 refractive index set to zero. This simulated bare plasmon

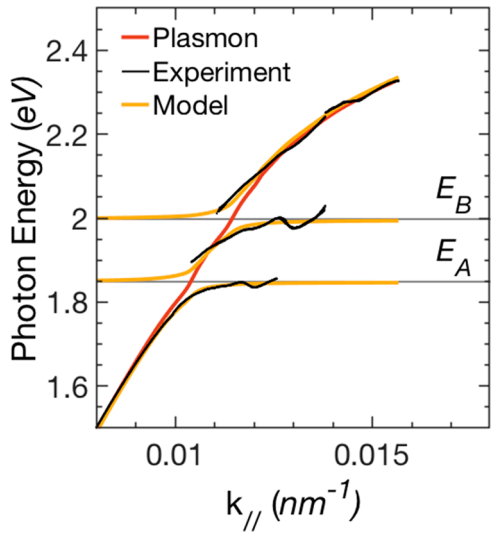

Figure 3. Semiclassical coupled oscillator model fit: Black data are peaks of the three hybrid modes taken from the experimental dispersion. Red data are peaks from the modeled uncoupled plasmon. Orange lines are the coupled harmonic oscillator fit to the black data. The gray lines labeled E_A and E_B are the uncoupled exciton positions, as fit by the model. Anticrossing of the three hybrid modes is a clear indication of a strongly coupled system.

https://dx.doi.org/10.1021/acsphotonics.0c00233
ACS Photonics 2020, 7, 1129–1134

dispersion is fitted to a single Lorentzian at each k-point and the peak value represents $E_{SPP}(k_{||})$ in the Hamiltonian and is plotted in Figure 3 as the red curve. See Figure S5 for a comparison between the experimental dispersion of the control Ag and the modeled dispersion with lossless MoS_2.

The three k-dependent eigenvalues of the Hamiltonian represent the three coupled modes of the system and thus the three branches of the dispersion. A least-squares fitting routine is used to fit these eigenvalues to the experimental data (in black), shown as the orange lines in Figure 3. The best fit Rabi splittings are 65 and 72 meV at the A- and B-exciton energy positions, respectively, which underestimate the experimentally observed values of 81 and 93 meV. The fit A- and B-exciton energies are 1.85 and 2.00 eV, in good agreement with the experimentally determined values of 1.86 and 2.01 eV.

Each of the three coupled modes is a quantum superposition of the uncoupled modes, each coherently exchanging energy at the Rabi frequency. The three eigenvectors, $|\phi\rangle_k$, of eq 1 can be expressed in the basis of the uncoupled plasmon, $|SPP\rangle$, A-exciton, $|A\rangle$, and B-exciton, $|B\rangle$, modes, shown in eq 2, with the square modulus of their respective coefficients, $|c_n|^2$, giving the contribution of each uncoupled mode to the final state. Figure 4a shows the Hopfield[38] coefficients for each of the three branches.

$$|\phi\rangle_k = c_1|SPP\rangle + c_2|A\rangle + c_3|B\rangle \quad (2)$$

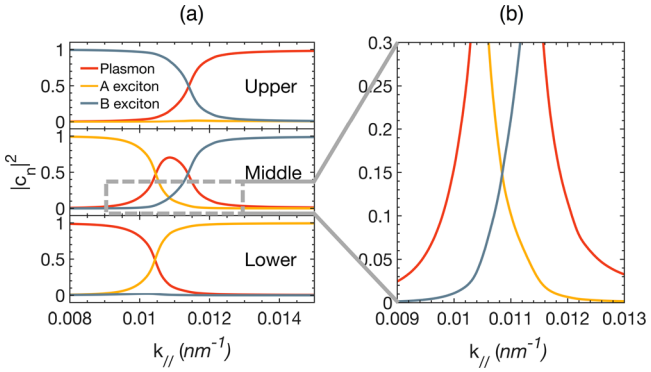

Figure 4. (a) Mixing coefficients for each of the three hybrid mode dispersion branches, as a function of transverse wavevector. The coefficients are obtained from the coupled harmonic oscillator model. (b) Mixing coefficients of the middle branch showing overlap of A- and B-excitons, implying coherent quantum superposition of the two modes, mediated by strong coupling to the plasmon.

At the limits of low energy and $k_{||}$ (lower branch) and high energy and $k_{||}$ (upper branch), the modes are purely plasmonic in nature, as the energies are far from the exciton energies. In the lower and upper branches at the crossing points of the uncoupled plasmon and exciton momenta, the modes are half plasmonic, half excitonic in nature. The lower branch contains no contribution from the B-exciton and the upper branch none from the A. Interestingly, the middle branch contains non-negligible contributions from both the A- and B-excitons (15% each at their intersection), indicating the excitons and plasmon are coherently hybridized and this hybridization is mediated by the plasmon. Such polariton-mediated exciton−exciton hybridization has been previously observed in cavities coupled with organic molecules[39] or to multiple material systems.[40,41] More recently polariton-mediated exciton−exciton and exciton−trion hybridization has been shown in the TMDCs at cryogenic temperatures.[28,42,43] Vasilevskiy et al. predicted room temperature hybridization of the A- and B-excitons in both MoS_2 and WS_2 (monolayers in photonic cavities).[37] Our observation confirms the predictions of Vasilevskiy et al. in MoS_2 and is the first at room temperature in any of the 2D TMDCs.

The coherent exciton−exciton hybridization presents an interesting question: how do the hybridized excitons influence the properties of the valley-polarized carriers in MoS_2? Monolayer, odd numbers of FL-MoS_2, and electrically gated even numbers of FL-MoS_2 exhibit broken inversion symmetry that leads to energy-degenerate spin-polarized valleys in the corners of the first Brillouin zone for both A- and B-excitons.[44−46] The valley-polarization lifetime of the A-exciton is enhanced under strong coupling, where the coherent exchange between A-exciton and polariton modes outcompetes decoherent scattering through mechanisms such as the Coulombic electron−hole exchange interaction.[44,47,48] Tokman et al. proposed that intervalley A-exciton entanglement should be possible by coupling linearly polarized single photons to exciton−polaritons in TMDCs.[49] The additional degree of freedom provided by the B-exciton motivates further study of the valley physics of the 2D TMDCs under strong coupling.

Finally, the transfer matrix method was used to study exciton−plasmon coupling combinatorially in the exciton−plasmon MX_2−P system, where M = (Mo, W), X = (S, Se), and P = (Ag, Au, Al, Cu). In Figure 5, Rabi splitting is clearly

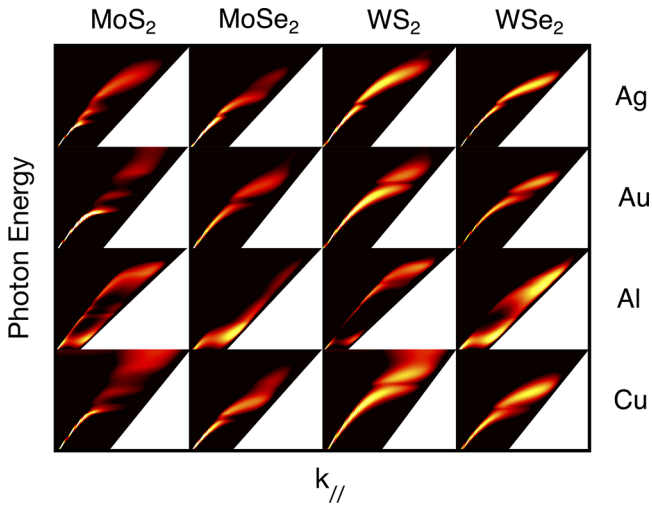

Figure 5. Generalized strong plasmonic coupling in 2D TMDC systems. A transfer matrix model is used and the thickness of each film is tuned to give the largest splitting. Rabi splitting is evident for each system except those with Al, where interpretation is more difficult. The axes are scaled to show the major features of the coupling near the A-exciton. Axis values are omitted for clarity; Figure S4 is fully labeled.

seen in each system, with the exception of Al. In Al, the plasmonic tuneability is limited to energies greater than ∼1.8 eV and sharp resonances only available at higher energies, limiting strong coupling in the TMDCs studied here. The TMDCs were modeled with few-layer thickness, which as noted above, is necessary to achieve large Rabi splitting at the A- and B-excitons.

The results in Figure 5 show that the Kretschmann-Raether method can be a useful platform for studies under strong

https://dx.doi.org/10.1021/acsphotonics.0c00233
ACS Photonics 2020, 7, 1129−1134

coupling conditions while varying other properties. For example, optical, electronic, and catalytic properties can be tuned by exchanging one metal or TMDC for another, while maintaining strong coupling. See the Supporting Information for details of the model and axis values.

In summary, we have reported room temperature strong coupling of the A- and B-excitons of MoS_2 with plasmons as well as exciton−exciton hybridization. Our room temperature findings represent an important advance in the field of strong coupling as they point to a new possible platform for studies on room temperature thresholdless lasing and quantum information processing. The reported A- and B-exciton hybridization motivates further study with possible applications such as intra- or intervalley quantum information transport and entanglement via exciton−exciton hybridization, controlled in an active strong coupling[50] device. Further, we demonstrate that the 2D TMDCs are a great platform for strong coupling studies in the Kretschmann-Raether configuration, allowing researchers wide latitude in their choice of plasmonic metal or TMDC. The Kretschmann-Raether method, with its open geometry, is conducive to biological and photoelectrochemical studies as well. While there has been much work on plasmonic biosensors, there has been little application of strong coupling to biology or chemistry, either of which could provide many opportunities for novel research.

METHODS

Sample Preparation. To fabricate the sample shown schematically in Figure 1a, Ag (40 nm) with a thin Ti adhesion layer (∼1 nm) was deposited on the hypotenuse of a right-angle glass prism (Edmund Optics) via electron beam deposition. FL-MoS_2 (∼5 nm) grown by chemical vapor deposition was transferred three consecutive times on top of the Ag for a total thickness of ∼15 nm.

Angle-Resolved Photoreflectance. The experimental dispersion curves were constructed from angle-resolved p-polarized reflectance spectra, taken through the glass side of the prism, as shown in Figure 1a. An ellipsometer (J. A. Woollam M-2000) was used to collect the data. The reflected light intensity was normalized to that of a control sample with 200 nm Ag on an identical prism, taken in the same manner. Thus, reflectance was calculated as $R(\lambda,\theta) = I(\lambda,\theta)/I_C(\lambda,\theta)$, where the intensity of the reflected light from the sample is I and from the control is I_C, and all data was taken spectroscopically at many angles.

ASSOCIATED CONTENT

Supporting Information

The Supporting Information is available free of charge at https://pubs.acs.org/doi/10.1021/acsphotonics.0c00233.

Sample preparation, measurement techniques, and modeling (PDF)

AUTHOR INFORMATION

Corresponding Authors

Aaron H. Rose − *Chemistry and Nanoscience Center, National Renewable Energy Laboratory, Golden, Colorado 80401, United States; Department of Physics, Boston College, Chestnut Hill, Massachusetts 02467, United States;* orcid.org/0000-0002-6603-8779; Email: aaron.rose@nrel.gov

Jao van de Lagemaat − *Chemistry and Nanoscience Center, National Renewable Energy Laboratory, Golden, Colorado 80401, United States; Renewable and Sustainable Energy Institute, University of Colorado at Boulder, Boulder, Colorado 80309, United States;* orcid.org/0000-0001-5851-6163; Email: jao.vandelagemaat@nrel.gov

Authors

Jeremy R. Dunklin − *Chemistry and Nanoscience Center, National Renewable Energy Laboratory, Golden, Colorado 80401, United States;* orcid.org/0000-0003-0070-8167

Hanyu Zhang − *Chemistry and Nanoscience Center, National Renewable Energy Laboratory, Golden, Colorado 80401, United States;* orcid.org/0000-0001-9942-8186

Juan M. Merlo − *Department of Physics, Boston College, Chestnut Hill, Massachusetts 02467, United States; Physics and Astronomy Department, Vassar College, Poughkeepsie, New York 12604, United States*

Complete contact information is available at: https://pubs.acs.org/10.1021/acsphotonics.0c00233

Author Contributions

The manuscript was written through contributions of all authors. All authors have given approval to the final version of the manuscript.

Notes

The authors declare no competing financial interest.

ACKNOWLEDGMENTS

We would like to thank Michael J. Naughton of Boston College for discussions and Sanjini U. Nanayakkara of NREL for assistance with AFM measurements. This work was authored in part by the National Renewable Energy Laboratory, operated by Alliance for Sustainable Energy, LLC, for the U.S. Department of Energy (DOE) under Contract No. DE-AC36-08GO28308. Funding provided by DOE Office of Science, Office of Basic Energy Sciences, Division of Chemical Sciences, Geosciences, and Biosciences, Solar Photochemistry Program. The views expressed in the article do not necessarily represent the views of the DOE or the U.S. Government. Juan M. Merlo acknowledges Vassar College for startup funding number ST000057.

REFERENCES

(1) Wang, Q. H.; Kalantar-Zadeh, K.; Kis, A.; Coleman, J. N.; Strano, M. S. Electronics and optoelectronics of two-dimensional transition metal dichalcogenides. *Nat. Nanotechnol.* **2012**, *7*, 699−712.

(2) Lu, Q.; Yu, Y.; Ma, Q.; Chen, B.; Zhang, H. 2D Transition-Metal-Dichalcogenide-Nanosheet-Based Composites for Photocatalytic and Electrocatalytic Hydrogen Evolution Reactions. *Adv. Mater.* **2016**, *28*, 1917−1933.

(3) Splendiani, A.; et al. Emerging Photoluminescence in Monolayer MoS_2. *Nano Lett.* **2010**, *10*, 1271−1275.

(4) Wang, H.; et al. Integrated Circuits Based on Bilayer MoS_2 Transistors. *Nano Lett.* **2012**, *12*, 4674−4680.

(5) Sanvitto, D.; Kéna-Cohen, S. The road towards polaritonic devices. *Nat. Mater.* **2016**, *15*, 1061−1073.

(6) Berman, P. R. *Cavity Quantum Electrodynamics*; Academic Press, 1994.

(7) Yokoyama, H. Physics and Device Applications of Optical Microcavities. *Science* **1992**, *256*, 66−70.

(8) Christopoulos, S.; et al. Room-Temperature Polariton Lasing in Semiconductor Microcavities. *Phys. Rev. Lett.* **2007**, *98*, 126405.

(9) Byrnes, T.; Kim, N. Y.; Yamamoto, Y. Exciton−polariton condensates. *Nat. Phys.* **2014**, *10*, 803−813.

(10) Khitrova, G.; Gibbs, H. M.; Kira, M.; Koch, S. W.; Scherer, A. Vacuum Rabi splitting in semiconductors. *Nat. Phys.* **2006**, *2*, 81−90.
(11) Cao, E.; Lin, W.; Sun, M.; Liang, W.; Song, Y. Exciton-plasmon coupling interactions: from principle to applications. *Nanophotonics* **2018**, *7*, 145−167.
(12) Hennessy, K.; et al. Quantum nature of a strongly coupled single quantum dot−cavity system. *Nature* **2007**, *445*, 896−899.
(13) Törmä, P.; Barnes, W. L. Strong coupling between surface plasmon polaritons and emitters: a review. *Rep. Prog. Phys.* **2015**, *78*, 013901.
(14) Reithmaier, J. P.; et al. Strong coupling in a single quantum dot−semiconductor microcavity system. *Nature* **2004**, *432*, 197.
(15) Hutchison, J. A.; Schwartz, T.; Genet, C.; Devaux, E.; Ebbesen, T. W. Modifying Chemical Landscapes by Coupling to Vacuum Fields. *Angew. Chem., Int. Ed.* **2012**, *51*, 1592−1596.
(16) Wiederrecht, G. P.; Hall, J. E.; Bouhelier, A. Control of Molecular Energy Redistribution Pathways via Surface Plasmon Gating. *Phys. Rev. Lett.* **2007**, *98*, 083001.
(17) Azarova, N.; et al. Coupling between a Molecular Charge-Transfer Exciton and Surface Plasmons in a Nanostructured Metal Grating. *J. Phys. Chem. Lett.* **2013**, *4*, 2658−2663.
(18) Agranovich, V. M.; Malshukov, A. G. Surface polariton spectra if the resonance with the transition layer vibrations exist. *Opt. Commun.* **1974**, *11*, 169−171.
(19) Pockrand, I.; Swalen, J. D. Anomalous dispersion of surface plasma oscillations. *J. Opt. Soc. Am.* **1978**, *68*, 1147−1151.
(20) Vasa, P.; Lienau, C. Strong Light−Matter Interaction in Quantum Emitter/Metal Hybrid Nanostructures. *ACS Photonics* **2018**, *5*, 2−23.
(21) Wurtz, G. A.; et al. Molecular Plasmonics with Tunable Exciton−Plasmon Coupling Strength in J-Aggregate Hybridized Au Nanorod Assemblies. *Nano Lett.* **2007**, *7*, 1297−1303.
(22) Gómez, D. E.; Vernon, K. C.; Mulvaney, P.; Davis, T. J. Surface Plasmon Mediated Strong Exciton−Photon Coupling in Semiconductor Nanocrystals. *Nano Lett.* **2010**, *10*, 274−278.
(23) Kittel, C. *Introduction to Solid State Physics*; John Wiley & Sons, Inc., 1986; Chapter 11.
(24) Gurioli, M.; et al. Well-width and aluminum-concentration dependence of the exciton binding energies in GaAs/$Al_xGa_{1-x}As$ quantum wells. *Phys. Rev. B: Condens. Matter Mater. Phys.* **1993**, *47*, 15755−15762.
(25) Liu, X.; et al. Strong light−matter coupling in two-dimensional atomic crystals. *Nat. Photonics* **2015**, *9*, 30−34.
(26) Schneider, C.; Glazov, M. M.; Korn, T.; Höfling, S.; Urbaszek, B. Two-dimensional semiconductors in the regime of strong light-matter coupling. *Nat. Commun.* **2018**, *9*, 2695.
(27) Dufferwiel, S.; et al. Exciton−polaritons in van der Waals heterostructures embedded in tunable microcavities. *Nat. Commun.* **2015**, *6*, 8579.
(28) Liu, W.; et al. Strong Exciton−Plasmon Coupling in MoS_2 Coupled with Plasmonic Lattice. *Nano Lett.* **2016**, *16*, 1262−1269.
(29) Low, T.; et al. Polaritons in layered two-dimensional materials. *Nat. Mater.* **2017**, *16*, 182−194.
(30) Pockrand, I.; Brillante, A.; Möbius, D. Exciton−surface plasmon coupling: An experimental investigation. *J. Chem. Phys.* **1982**, *77*, 6289−6295.
(31) Bellessa, J.; Bonnand, C.; Plenet, J. C.; Mugnier, J. Strong Coupling between Surface Plasmons and Excitons in an Organic Semiconductor. *Phys. Rev. Lett.* **2004**, *93*, 036404.
(32) Kretschmann, E.; Raether, H. Radiative Decay of Non Radiative Surface Plasmons Excited by Light. *Z. Naturforsch., A: Phys. Sci.* **1968**, *23a*, 2135−2136.
(33) Rose, A. H. RTACalc, version 1.0; 2018. https://github.com/rose3fa/RTACalc (accessed June 1, 2019).
(34) Balci, S.; et al. Tuning surface plasmon-exciton coupling via thickness dependent plasmon damping. *Phys. Rev. B: Condens. Matter Mater. Phys.* **2012**, *86*, 235402.
(35) Symonds, C.; et al. Particularities of surface plasmon−exciton strong coupling with large Rabi splitting. *New J. Phys.* **2008**, *10*, 065017.
(36) Liu, W.; et al. Understanding the Different Exciton−Plasmon Coupling Regimes in Two-Dimensional Semiconductors Coupled with Plasmonic Lattices: A Combined Experimental and Unified Equation of Motion Approach. *ACS Photonics* **2018**, *5*, 192−204.
(37) Vasilevskiy, M. I.; Santiago-Pérez, D. G.; Trallero-Giner, C.; Peres, N. M. R.; Kavokin, A. Exciton polaritons in two-dimensional dichalcogenide layers placed in a planar microcavity: Tunable interaction between two Bose−Einstein condensates. *Phys. Rev. B: Condens. Matter Mater. Phys.* **2015**, *92*, 245435.
(38) Hopfield, J. J. Theory of the Contribution of Excitons to the Complex Dielectric Constant of Crystals. *Phys. Rev.* **1958**, *112*, 1555−1567.
(39) Holmes, R. J.; Forrest, S. R. Strong Exciton-Photon Coupling and Exciton Hybridization in a Thermally Evaporated Polycrystalline Film of an Organic Small Molecule. *Phys. Rev. Lett.* **2004**, *93*, 186404.
(40) Gómez, D. E.; Vernon, K. C.; Mulvaney, P.; Davis, T. J. Coherent superposition of exciton states in quantum dots induced by surface plasmons. *Appl. Phys. Lett.* **2010**, *96*, 073108.
(41) Flatten, L. C.; Coles, D. M.; He, Z.; Lidzey, D. G.; Taylor, R. A.; Warner, J. H.; Smith, J. M. Electrically tunable organic−inorganic hybrid polaritons with monolayer WS2. *Nat. Commun.* **2017**, *8*, 14097.
(42) Wang, Q.; et al. Direct observation of strong light-exciton coupling in thin WS_2 flakes. *Opt. Express* **2016**, *24*, 7151−7157.
(43) Cuadra, J.; et al. Observation of Tunable Charged Exciton Polaritons in Hybrid Monolayer WS_2−Plasmonic Nanoantenna System. *Nano Lett.* **2018**, *18*, 1777−1785.
(44) Schaibley, J. R.; Yu, H.; Clark, G.; Rivera, P.; Ross, J. S.; Seyler, K. L.; Yao, W.; Xu, X. Valleytronics in 2D materials. *Nat. Rev. Mater.* **2016**, *1*, 16055.
(45) Li, Y.; et al. Probing Symmetry Properties of Few-Layer MoS_2 and h-BN by Optical Second-Harmonic Generation. *Nano Lett.* **2013**, *13*, 3329−3333.
(46) Wu, S.; et al. Electrical tuning of valley magnetic moment through symmetry control in bilayer MoS_2. *Nat. Phys.* **2013**, *9*, 149−153.
(47) Chen, Y.-J.; Cain, J. D.; Stanev, T. K.; Dravid, V. P.; Stern, N. P. Valley-polarized exciton−polaritons in a monolayer semiconductor. *Nat. Photonics* **2017**, *11*, 431−435.
(48) Dufferwiel, S.; et al. Valley-addressable polaritons in atomically thin semiconductors. *Nat. Photonics* **2017**, *11*, 497−501.
(49) Tokman, M.; Wang, Y.; Belyanin, A. Valley entanglement of excitons in monolayers of transition-metal dichalcogenides. *Phys. Rev. B: Condens. Matter Mater. Phys.* **2015**, *92*, 075409.
(50) Lee, B.; et al. Electrical Tuning of Exciton−Plasmon Polariton Coupling in Monolayer MoS_2 Integrated with Plasmonic Nanoantenna Lattice. *Nano Lett.* **2017**, *17*, 4541−4547.

https://dx.doi.org/10.1021/acsphotonics.0c00233
ACS Photonics 2020, 7, 1129−1134